ELSEVIER

International Journal of Mass Spectrometry 189 (1999) 103–113

International Journal of Mass Spectrometry

Study of the electron ion recombination in high pressure flowing afterglow: recombination of $NH_4^+.(NH_3)_2$

J. Glosík*, G. Bánó, R. Plašil, A. Luca, P. Zakouřil

Department of Electronics and Vacuum Physics, Mathematics and Physics Faculty, Charles University, V Holešovičkách 2, Prague 8, Czech Republic

Received 14 December 1998; accepted 7 April 1999

Abstract

Rate coefficients for the dissociative recombination of O_2^+ and $NH_4^+.(NH_3)_2$ with electrons have been measured using the high pressure flowing afterglow (HPFA) technique. The electron energy distribution function, effective temperature, and electron number density of the recombination dominated plasma have been measured by a Langmuir probe at pressures up to 11 Torr. The measured value of the recombination rate coefficient of O_2^+ was used for validation of the Langmuir probe measurements at medium pressures. It is found that the recombination rate coefficient of the recombination of the cluster $NH_4^+.(NH_3)_2$ ion is 1.4×10^{-6} cm^3 s^{-1} at 600 K. (Int J Mass Spectrom 189 (1999) 103–113) © 1999 Elsevier Science B.V.

Keywords: Electron ion recombination; Recombination of cluster ions; Langmuir probe; Flowing afterglow; Recombination coefficient

1. Introduction

Dissociative recombination of electrons with positive molecular ions is an important loss process for electrons and ions in electron/ion plasmas. The elementary process of recombination occurs in a single collision of electron and molecular cations in a certain quantum state and, at a given relative velocity (v) is characterized by the cross section $\sigma(v)$. Recombination in multiple collision systems under conditions of thermodynamic equilibrium at temperature (T) is characterized by the recombination rate coefficient $\alpha(T)$. This definition in experimental studies is quite often extended by an assumption that "electron gas" and "ion gas" are in quasiequilibrium characterized by temperatures T_e and T_+, respectively. In low temperature plasmas T_+ is usually equal to the temperature of the neutral gas (T_g), and the electron energy distribution function (EEDF) is close to Maxwellian distribution. In general $T_e \neq T_+$ and very often $T_e \gg T_+$. The recombination rate coefficient in such nonthermal plasmas are then given as a function of T_e, $\alpha_e(T_e)$. The difference between $\alpha_e(T_e)$ and $\alpha(T)$ is sensitive to the dependence of the recombination process on the internal energy of the recombining ions. In the case of an experimental determination of α it is important to consider how close we are to these "ideal conditions." This is also important for applying $\sigma(v)$ or $\alpha(T)$ to describe processes occurring in a real plasma.

The electron ion recombination has been studied for many years by a variety of techniques. These studies can be divided into two types of experiments: single and multiple collision systems. In the single

* Corresponding author. E-mail: juraj.glosik@mff.cuni.cz

PII S1387-3806(99)00058-5

collision techniques the cross section is usually measured at a particular kinetic energy of the recombining particles. These techniques usually use beams of monoenergetic electrons (or negative ions) and positive ions (in a defined quantum state if possible). In the multiple collision plasma techniques, usually afterglow techniques, the recombination rate coefficient is determined from a decay of the recombination dominated plasma of a particular composition. The majority of available recombination rate coefficients and cross sections were obtained using experiments from one of these two groups. In a few cases the products of the recombination and their internal energy are also determined [1–4]. The most productive of the afterglow techniques are the stationary afterglow method (SA, see, e.g. the review by Johnsen [5]) and the flowing afterglow method (FA, see e.g. [6]). To obtain the recombination rate coefficient from an afterglow experiment it is necessary to know the absolute value of the electron number density (n_e) and the ion number density (n_+) in the recombining plasma. The plasma is usually quasineutral, i.e. $n_e = n_+ = n$, at number densities of the charged particles used in these experiments. A variety of methods for determination of the absolute value of the electron number density were used in SA studies, e.g. microwave cavity, Langmuir probe, detection of the emission of the photons, etc. The experiments using microwaves usually give the data averaged over a certain volume of plasma and in order to obtain n_e it is necessary to know the geometrical configuration of the electric field and to assume a particular spatial distribution of charged particles. A Langmuir probe measures the local value of n_e and, usually, both time and spatial distributions of n_e can be obtained. A very successful technique for studying recombination work involves the use of a FA equipped with a Langmuir probe, denoted as FALP (flowing afterglow Langmuir probe) and its extension, FALP-MS (with movable mass spectrometer [7]).

Many recombination rate coefficients have been measured during the last 30 years but there is still a lack of experimental data concerning recombination of the cluster ions [8]. The fast formation of the cluster ions prior to recombination requires a high pressure of the buffer gas to enhance three-body association reactions in which these clusters are formed. Because of this lack of data on the recombination of cluster ions we have built the flow tube working at pressures of the buffer gas ranging from 1 to over 20 Torr (HPFA = high pressure flowing afterglow [9]). The main problem connected with the relatively high operational pressure is that there is no simple theory that would be easily applicable for the calculation of n_e from the probe characteristic at pressures higher than 1 Torr (in this context we will call these pressures “medium pressures”).

Because of the large ratio of the masses of the ions (m_+) and the electrons (m_e), “electron gas” and “ion gas” thermalize (relax) in the afterglow with different time constants. It was demonstrated several times that the afterglow plasma is not necessarily completely thermalyzed and the EEDF often departs from Maxwellian distribution in the beginning of the recombination region. Slow relaxation in Ar was successfully used in the study of the electron temperature dependence of attachment [10]. The recombination coefficient is sensitive to the collision energy of the recombining electron and ion. For small molecular ions the rate of the recombination generally decreases with increasing collision energy (temperature), and as a consequence the slow electrons are selectively removed from such recombination dominated plasma. If the re-Maxwellianization is not effective enough, the EEDF can then be different from the Maxwellian distribution. In the flowing afterglow plasma the electron gas can also be influenced by the high value of the gradient of the plasma potential corresponding to the fast decrease of the number density of the charged particles along the flow tube due to their recombination. Particularly, this can happen in an afterglow dominated by very fast recombination of cluster ions and sufficient concentration of the plasma ($>10^9$ cm^{-3}). Because of that possibility, the EEDF and T_e (if the EEDF is Maxwellian or very close to Maxwellian) have to be measured. We have studied the plasma relaxation in the Ar buffered flowing afterglow and we found that it can take several milliseconds for T_e to approach 300 K at 0.5 Torr [11]. This means that the electron gas is not fully

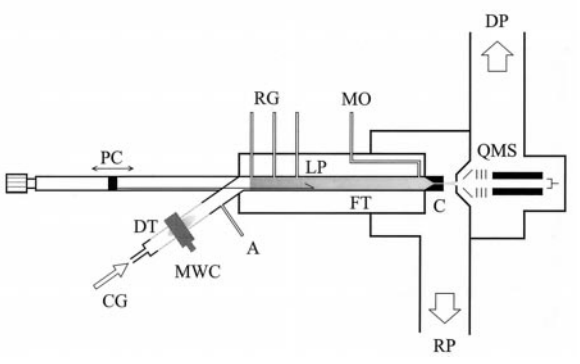

Fig. 1. HPFA—High pressure flowing afterglow; CG—carrier gas; A—Ar entry port; MWC—microwave cavity; DT—discharge tube; FT—flow tube; C—capillary; RG—reactant gas entry ports; QMS—quadrupole mass spectrometer; PC—probe control; LP—Langmuir probe; RP—Roots pump; DP—diffusion pump.

thermalized during the recombination controlled decay of the plasma. The slow relaxation in Ar buffer is a consequence of the low cross section for the elastic collisions of near thermal electrons with Ar due to the Ramsauer effect [12] and a large ratio of the masses of Ar and electrons. The relaxation of an electron gas is relatively faster in the He buffer because of the higher cross section of elastic scattering and smaller mass of helium atoms [13]. Simultaneous measurements of plasma number density and EEDF were reported in several recent publications [10,14–17]. The relaxation of the afterglow plasma can also be influenced by the presence of very energetic neutral particles—atoms in metastable electronic states. This problem is usually solved by the addition of a small percentage of gas that removes the metastables by Penning ionization, e.g. addition of Ar to He buffered FA [18]. In the Appendix we demonstrated how energetic electrons produced in Penning ionization can disturb the relaxation process and the EEDF in the flowing afterglow. The presence of the reactant gases used for formation of particular ions can also influence the EEDF. Usually, the relaxation is faster in the presence of molecular gases due to inelastic collisions that absorb the energy of the electrons with higher efficiency. There is a lack of experimental studies of the parameters of these processes (see e.g. the study of the relaxation of the EEDF in flowing afterglow in the presence of *n*-hexan and benzene in [16]).

The goal of the present study is to measure the recombination rate coefficients of cluster ions with electrons with a precise specification of the plasma parameters. In the present study the well established value of α for dissociative recombination of O_2^+ with electrons and its electron temperature dependence [19] is used for "calibration" of the probe at helium pressures from 3–11 Torr. Calibration validation of the probe reduces inaccuracies in determining the electron number density and thus improves accuracy in determining the recombination rate coefficients.

2. Experiment

The FALP technique and its HPFA variation have been described previously [9], so only a short description will be given. A diagram of the HPFA apparatus is given in Fig. 1. The actual flow tube is made from stainless steel (internal diameter is 18 mm) with a short glass upstream section. High purity He (grade 5.0) was used as a buffer. The carrier gas in the present experiment is further purified in the liquid nitrogen trap filled with molecular sieves. The impurities (O_2, N_2, H_2O) are thus reduced to a few parts per million. The mass spectrometer at the downstream part of the flow tube, coupled via a capillary and a differentially pumped chamber, is used to monitor the relative number densities of the ions. The ions flowing from the capillary are attracted by a small negative potential through the differentially pumped chamber towards a conical input electrode with a sampling orifice. The applied potential difference is very small in order to exclude collisional dissociation of the detected cluster ions. The axially movable Langmuir probe (used for measurement of the electron number density) is 14 micrometers in diameter and 4 mm long. The probe characteristics are measured using a 12 bit A/D convertor in the equidistant steps of the probe voltage provided by a 12 bit D/A convertor. From these probe characteristics the ion part of the probe current, I_+, is first calculated by extrapolation of the ion "saturated current" towards plasma potential. The electron current to the probe, I_e, is then obtained by subtracting I_+ from the total probe

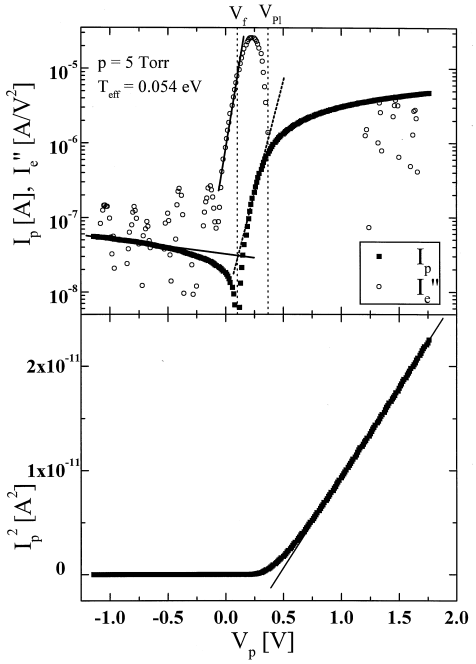

Fig. 2. Upper panel: the measured probe characteristic. From the slope of the linear part (dashed line) of the semilogarithmic plot of the second derivative of the electron current the effective temperature, T_{eff}, is calculated. Plasma potential V_{Pl} is given by the inflex point of the probe characteristic, I''_e is changing its sign at this potential of the probe. The floating potential V_f is the potential at which the probe current changes its sign. The probe current at $V_p < V_f$ ("saturated ion current") is plotted with the same sign as the electron part in order to plot it in the logarithmic scale. Lower panel: the plot of the square of the probe current (I_p^2) vs. probe potential (V_p). The electron number density is calculated from the slope of the linear increasing part of the plot (saturated electron current). The pressure of the buffer gas $p = 5$ Torr.

current. A second derivative against probe potential (V_P) is then calculated from I_e, which finally leads to the EEDF [17,20]. The plasma potential V_{Pl} is determined from the inflection point of the probe characteristic. If the EEDF is Maxwellian, the semilogarithmic plot of d^2I_e/dV_P^2 against V_P is for $(V_P–V_{\text{Pl}}) < 0$ linear and from the slope of this plot the electron temperature, T_e, can be calculated (see Fig. 2 for an example). The electron temperature can also be obtained from the slope of the semilogarithmic plot of the probe characteristic (see dashed line in Fig. 2). In the case of a deviation of the EEDF from the Maxwellian distribution, these two "experimental" temperatures can differ because they characterize different parts of the energy distribution of the electrons. In the present work the electron number densities were obtained from the "saturated part" of the probe current at positive voltage on the probe $(V_P–V_{\text{Pl}}) > 0$ [20], see lower panel of Fig. 2. We will demonstrate that this method gives valid data on the measurement of the rate coefficient of recombination of O_2^+ with electrons. The plasma is generated by microwave discharge in the upstream glass part of the flow tube and it is carried along the flow tube by the flow of He. Because of the high buffer gas pressure, the He^+ ions formed in the discharge are converted in the three-body association to He_2^+ immediately after the discharge region. Ar is added to the flow tube shortly after the discharge in order to remove metastables. In the fast dissociative charge transfer (with the rate coefficient 2×10^{-10} cm^3 s^{-1}) the He_2^+ ions are then reacting with Ar forming Ar^+ ions, which are thus the dominant ion specie in the flow tube downstream of the Ar entry port. The rate coefficients of the ion molecule reactions taking part in this post-discharge and "pre-reaction" part of the flow tube are known and hence it was possible to calculate plasma composition by solving balance equations using the initial value of the n_e at $L = 0$. The evolutions thus obtained are plotted in Fig. 3. The number density of the helium metastables is obtained from the measured increase of the electron number density due to Penning ionization after the addition of Ar (see Appendix for details). The evolutions of the electron concentration (n_e) and electron temperature (T_e) along the flow tube in the mixture of He and Ar (~1% of Ar) are plotted in Fig. 4. Here $L = 0$ corresponds to the second entry port where the second reactant (O_2 or NH_3 in the present experiment) is added. The recombination of the atomic ions is very slow and the plasma is diffusion dominated. Note that $T_e = 0.03$–0.04 eV (corresponding to ~300 K). The linear decay of n_e in the semilogarithmic plot indicates that the diffusion is governing the decay of the plasma. Because of the destruction of the He metastables the electron temperature is already relaxed to buffer gas temperature, but without addition of Ar T_e is 600 K. The obtained $T_e \sim 300$ K shows high accuracy of the

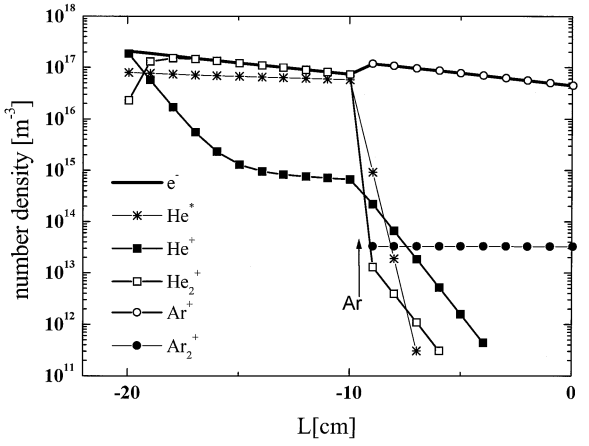

Fig. 3. The calculated evolution of the composition of the flowing afterglow plasma. The solution of the balance differential equations is fitted to the measured n_e at $L = 0$. The number density of the helium metastables is at $L = -20$ cm, correlating to the increase of the electron number density due to the Penning ionization after the addition of Ar at $L = -10$. The calculations are made for He buffer at pressure $p = 9.5$ Torr with the addition of Ar (~1%).

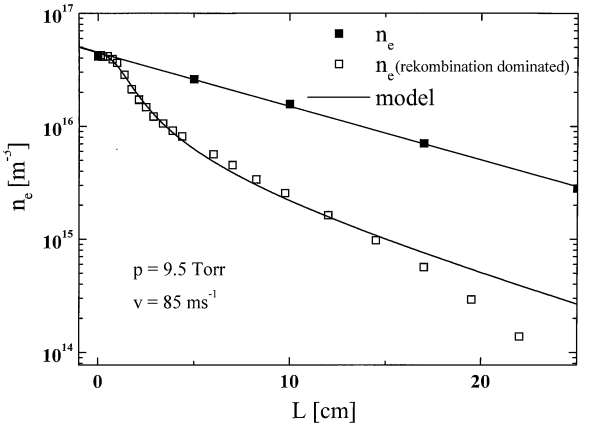

Fig. 4. The measured evolution of the electron number density, n_e (closed symbols), and the electron temperature, T_{eff} along the flow tube in the He afterglow with the addition of Ar (~1%) at $L = -10$ cm. The open symbols indicate data obtained after addition of O_2. The full lines correspond to the values calculated by the solution of the balance differential equations. The decay measured without addition of O_2 corresponds to the decay due to diffusion losses at a measured temperature. These are "zero" conditions for recombination studies. The buffer gas pressure $p = 9.5$ Torr.

measurements and demonstrates that the probe can be successfully used to study recombination in the flowing afterglow plasma in HPFA.

The plasma velocity (required for conversion of the axial position to time) was measured by pulse modulation of the discharge from the delay of the perturbation of the afterglow plasma for different positions along the flow tube. The plasma velocity is constant along the flow tube and has the value 50–80 ms^{-1} dependent on the actual diameter of the output capillary and pressure of He. The correlation between the plasma velocity and the bulk gas velocity of He was in agreement with previous flow tubes measurements. The accuracy of the measured recombination rate coefficient is ±30% as usual for the flowing afterglow experiments.

3. Results and discussion

3.1. Validation of the probe measurements

Before measuring the recombination coefficients of the cluster ions it was necessary to validate the Langmuir probe measurements at pressures higher than 1 Torr by measuring the rate coefficient of dissociative recombination of a simple diatomic ion. We have chosen O_2^+, for which the recombination coefficient is well established [19], and there is no evidence of any pressure dependence of its value. O_2^+ ions can be formed simply by adding O_2 into the relaxed plasma at $L = 0$. The binary reaction of the atomic ions (predominantly Ar^+) with O_2 ($k = 5 \times 10^{-11}$ cm^3 s^{-1} (see compilation in [21]) then ensures that, in the conditions of our experiment, 98% of the ions are converted to O_2^+ within 1 cm (the limitation is due to the finite rate of the mixing of O_2 with the buffer). The formed O_2^+ ions then undergo dissociative recombination with the plasma electrons. The electron number density measured along the flow tube after addition of O_2 is plotted in Figs. 4 and 5. The flat part at the beginning of the slope corresponds to the transition region, where O_2 is entering the flow tube and the atomic ions are converted to molecular O_2^+ ions, but the recombination is already substantial. The full line in Fig. 4 represents n_e, calculated by solving the balance equation when recombination and diffusion is considered (with $\alpha = 2 \times 10^{-7}$ cm^3 s^{-1} and

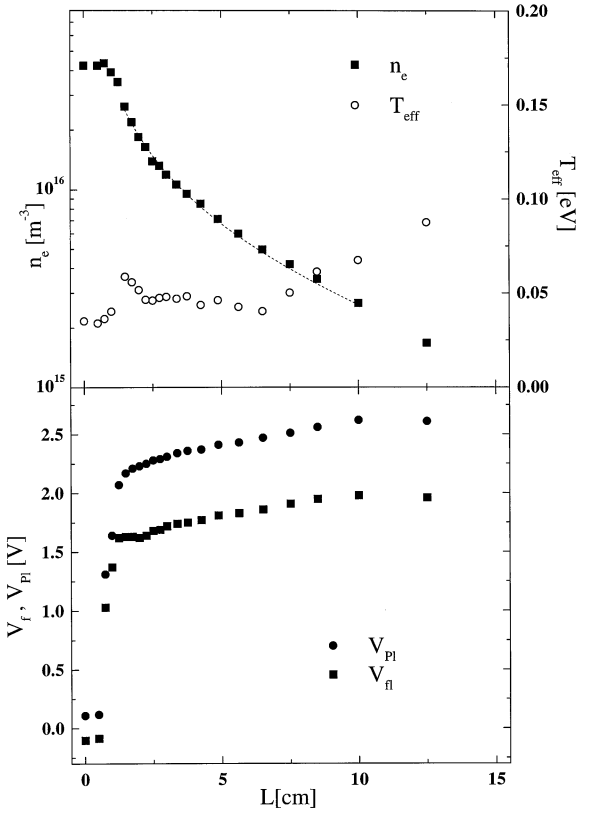

Fig. 5. Upper panel: the evolution of the electron number density after addition of O_2 at $L = 0$. The dashed line is the best fit of the experimental data according to Formula (1) for $L = 1.5$–10 cm. The open circles show evolution of the T_{eff} along the flow tube (see explanation in the text). The pressure of the buffer gas $p = 11.2$ Torr, the plasma velocity $v = 88\ \text{ms}^{-1}$. Lower panel: the evolution of the plasma potential, V_{Pl} and of the floating potential, V_f, in the recombination controlled flowing afterglow plasma after the addition of O_2 at $L = 0$. Both potentials are measured against the potential of the metal body of the flow tube.

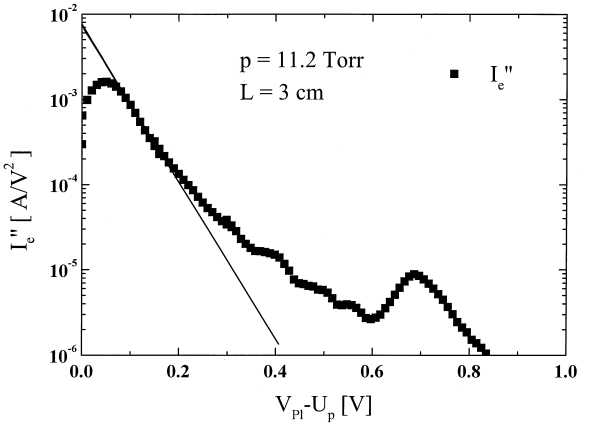

Fig. 6. The second derivative of the electron part of the probe current vs. the probe potential, dI_e^2/d^2V_P. In a semilogarithmic plot a second derivative of the probe current is linear if an EEDF is Maxwellian. The full line is the apparent linear fit of the data in the low energy part of the plot. From the fit T_{eff} is calculated. In the high energy part there is an excess of electrons in comparison with the Maxwell distribution characterized by a temperature equal to T_{eff}. At a very low value of the difference of the potentials between probe and plasma, $(V_{\text{Pl}}–V_p)$, accuracy of the probe data is very low and we cannot comment on the decline of the measured data in this region. The values of $(V_{\text{Pl}}–V_p)$ in the plot are numerically equal to corresponding energies of electrons in the EEDF given in eV.

$T_e = 0.03$ eV). Again, the calculation is normalized to the measured value of n_e at $L = 0$. The agreement of the measured and calculated data is very good. The deviation at $L > 15$ cm can be caused by the presence of negative ions or by the increase of the ambipolar diffusion due to the increase of T_e. In order to obtain the recombination rate coefficient, the experimental data for $L \geq 1.5$ cm were fitted by the function

$$n_e = \left[\alpha \frac{\exp(\nu_D t) - 1}{\nu_D} + \frac{1}{n_{e0}} \exp(\nu_D t) \right]^{-1} \qquad (1)$$

which describes losses of electrons by both diffusion (characterized by ν_D) and by recombination (characterized by α). n_{e0} is the electron number density at $L = 0$ (corresponding to time $t = 0$). The Function (1) is the analytical solution of the balance equation with diffusion and recombination loss terms only. The fit of the data is plotted by a dashed line in Fig. 5 (upper panel). Because of the rapid change of n_e in the region $L = 0$–1.5 cm, the plasma potential V_{Pl} and the floating potential V_f change very rapidly and the intensity of the electric field, E, is very high (1–2 V/cm), see lower panel of Fig. 5. This high E influences the EEDF, as is indicated by the measurements of the EEDF in this region, showing substantial deviation from the Maxwellian distribution. The EEDF relaxed within 1.5 cm (~0.2 ms) to a distribution close to Maxwellian. The second derivative of the electron part of the probe current versus the probe potential taken at $L = 3$ cm is plotted in Fig. 6. The linear part of the semilogarithmic plot (fitted by the apparent linear fit) indicates that the body of the

EEDF is close to Maxwellian, but the high energy part of the EEDF is distorted. Effective temperature T_{eff} was calculated from the low energy part of the EEDF, which is close to Maxwellian. Similar behavior of the EEDF was also observed for other positions in the flow tube and for other pressures of He. The deviation of the measured data from the straight line at very low (V_{Pl}–V_p) is caused by effects on the surface of the probe and by fluctuation of the potential of the plasma. These effects influence probe current at probe potential very close to plasma potential (<0.1 V). There is an excess of electrons in the high energy part of the EEDF, indicating the presence of a source of energetic electrons. The energy is "flowing" from the high energy part of the EEDF to the low energy part, thus eventually elevating T_{eff} above 300 K. The effective temperature, T_{eff}, obtained from the measured EEDF is plotted in Fig. 5. Note the low value $T_{\text{eff}} = 0.03$ eV before the recombination region (at $L = 0$) and the increase of T_{eff} up to 0.06 eV at $L = 1.5$ cm. We assume that the increase is related to the high value of E and to fast removal of slow electrons by recombination. E is decreasing at $L \geq 1.5$ cm and the temperature is also decreasing to $T_{\text{eff}} \sim 0.04$ eV at $L \sim 2.5$ cm for the data plotted in Fig. 5. At $L >$ 10 cm n_e is very small and accuracy of the determination of T_{eff} is low, also due partly to increasing deviation of the EEDF from the Maxwellian distribution. Usually it is assumed that plasma in the He buffer is relaxed within a few microseconds and that in the recombination region $T_e = 300$ K. From data plotted in Figs. 5 and 6 it is evident that in the real conditions, the relaxation of the recombination dominated plasma is not so simple. Two sets of the recombination rate coefficients are plotted in Fig. 7. In the first set (open symbols) the measured recombination rate coefficients were obtained with the assumption, commonly used in He FALP studies, that $T_e = 0.03$ eV (assuming that the electron gas is relaxed in the collisions with He atoms to the temperature of the buffer gas) are plotted. The second set (closed symbols) represents the recombination rate coefficients obtained with the assumption that the electron temperature can be characterized by T_{eff} obtained from the measured EEDF. The recombination of O_2^+ with

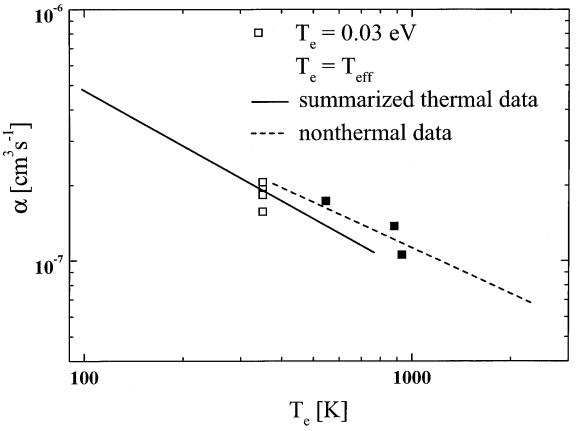

Fig. 7. The measured recombination rate coefficient (α) of the recombination of ions O_2^+ with electrons. The open symbols indicate the data if temperature of the electrons is assumed to be 300 K. The closed symbols indicate the recombination rate coefficient if T_{eff} obtained from measured data is taken as the temperature of electron gas. The full line represents summarization of "thermal" $\alpha(T)$ and the dashed line represents "nonthermal" $\alpha_e(T_e)$ data obtained in other experiments (see data and references [19]).

electrons and its temperature dependence was measured in many independent experiments; the obtained results can be summarized by the formula $\alpha = 2.10^{-7}\ (300/T_e)^{0.65}$, plotted by the full line in Fig. 7 [19]. Note the good agreement of our data with previous studies [22,23]. The present experiment utilizes this well established value of α for the validation of the probe at medium pressures. In both sets the accuracy of obtained recombination rate coefficients is within an ~30% limit. This indicates that the determination of the electron number density by the described method and the applied probe is in the pressure range 3–11 Torr correct to within ±30%.

3.2. Recombination of $NH_4^+.(NH_3)_2$

The ion–molecule reactions taking place in the formation of the $NH_4^+.(NH_3)_2$ ions are very fast [24] and in a very short time the ions reach equilibrium concentrations. The ionic composition depends only on the flow of ammonia. The results of our previous study of the reaction kinetics of the clustering reactions in the presence of ammonia in the flowing afterglow at 300 K [9] allow us to choose such a flow

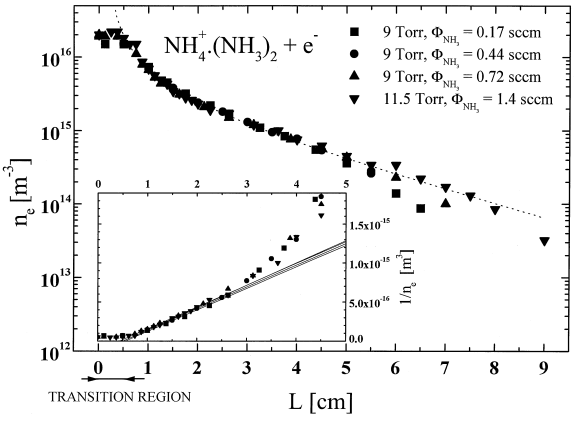

Fig. 8. The evolution of the electron number density n_e along the flow tube after addition of NH_3. The different flow rates of NH_3 and different pressures of the buffer gas are indicated by different symbols. The dotted line is the best fit of the all data points by Formula (a). The values $1/n_e$ for the same data are plotted in the insert. The full lines represent apparent linear fits.

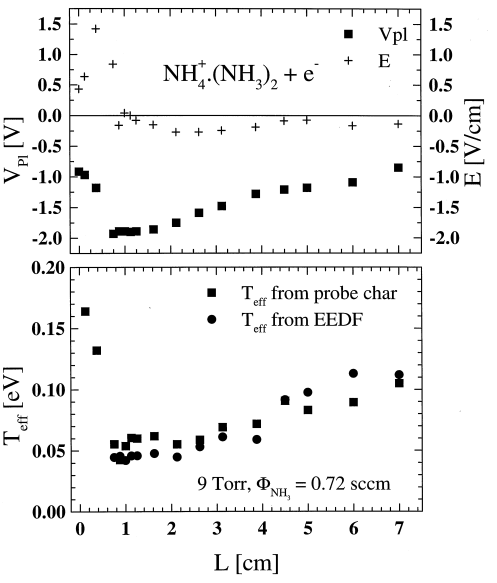

Fig. 9. Upper panel: the evolution of the plasma potential, V_{Pl}, and intensity of the electric field, E, along the flow tube in the recombination dominated plasma. Lower panel: the evolution of the effective temperature of the electrons along the flow tube; the data are obtained from the probe characteristic and also from the EEDF. The plots correspond to the data given in Fig. 8 taken at p = 9 Torr = 0.72 sccm.

of ammonia via the reactant port, that $NH_4^+.(NH_3)_2$ are the dominant ions in the upstream part of the flow tube (from 0.5 cm). Because the conversion from the atomic Ar^+ ions to $NH_4^+.(NH_3)_2$ cluster ions takes place at charged particle number densities $>10^{16}$ m^{-3}, the recombination

$$NH_4^+.(NH_3)_2 + e^- \xrightarrow{\alpha} \text{neutral products} \qquad (2)$$

starts to be the dominant loss process in this region immediately after the formation of the cluster ions. $NH_4^+.(NH_3)_2$ ions are formed within 1 cm from the ammonia entry inlet. The measurements were made for NH_3 flows from 0.17–1.4 sccm, which cover a broad range of NH_3 number densities, where $NH_4^+.(NH_3)_2$ is the dominant ion in the recombination region. The estimation made on the basis of our study of the equilibrium concentrations of the ions is that there is >80% of $NH_4^+.(NH_3)_2$ ions in the recombination dominated region. We assume that plasma is quasineutral and n_e characterizes both electron and positive ions number densities. The experimentally obtained evolution of the electron number density along the upstream part of the flow tube is plotted in Fig. 8. The decays of the electron number densities were determined at two different pressures and for four different flows of ammonia. Note that decays are independent of the pressure and the flow of ammonia. The linear part of the semilogarithmic plot of n_e (for $L > 3.5$ cm) corresponds to the region where diffusion is the dominant process. The recombination coefficient $\alpha = 1.4 \times 10^{-6}$ cm^3 s^{-1} was obtained by using Eq. (1) to fit the data; the best fit is indicated by a dotted line. The deviation at $L < 0.5$ cm corresponds to the introduction of the reactant gas and to the formation of the ionic clusters. The reciprocal values $(1/n_e)$ as a function of the position in the flow tube are plotted in the insert of Fig. 8. The linear part of the reciprocal plot corresponds to the region where recombination is the dominant process. The change of the electron number density due to the recombination is very dramatic as the electron number density falls to within 2 cm (corresponding decay time is <0.2 ms) by nearly one order of magnitude. The evolution of the plasma potential and the intensity of the electric field are plotted in the upper part of Fig. 9. The

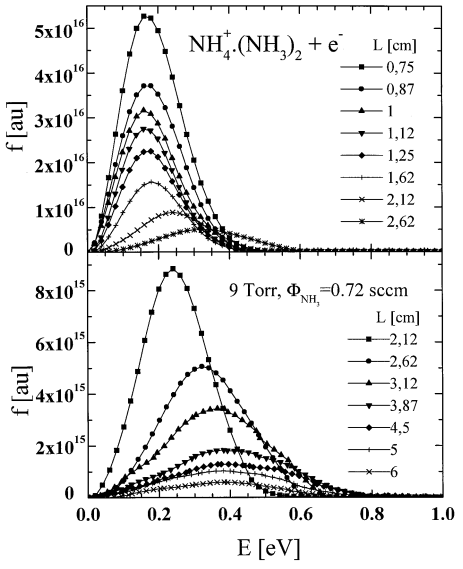

Fig. 10. The evolution of the EEDF along the flow tube. In the upper panel the EEDF in the recombination controlled region are plotted. The EEDF are normalized to the electron number density and are plotted in arbitrary units. The plots correspond to the data given in Figs. 8 and 9.

electron temperatures as determined from the probe characteristics and from the EEDF are plotted in the lower part of Fig. 9. The measured EEDF are plotted in Fig. 10. Note that in the region where recombination is dominant (L = 0.5–2.5 cm) the intensity of the electric field is close to zero and the electron temperature is nearly constant $T_e \sim 0.05$ eV. The EEDF in this region is close to a Maxwellian distribution and the T_e obtained by both methods are nearly the same. For $L > 2.5$ T_e starts to increase. The probe current is decreasing with L, as was already mentioned, due to the rapid decrease of n_e by the recombination and therefore the probe measurements at $L >$ 4 cm are less accurate than in the recombination controlled region at $L < 4$ cm.

The observation that T_e is elevated above 0.03 eV can be explained by preferential removal of the slow electrons from the distribution and possibly also by the influence of the relatively intense electric fields in the recombining plasma. Thus the measured value of the recombination coefficient $\alpha = 1.4 \times 10^{-6}$ cm^3 s^{-1} for the $NH_4^+.(NH_3)_2$ ions corresponds to T_e = 0.06 eV (equivalent to 600 K) and this has to be considered when comparing this value to the value from a previous stationary afterglow study of $\alpha = 2.7 \times 10^{-6}$ cm^3 s^{-1} that was obtained at T_e = 300 K (see [25] and compilation in [8]). This can indicate that the rate of the recombination of the cluster ions is decreasing with increasing T_e. Previous data on temperature dependence of recombination coefficients of recombination of cluster ions are not very accurate [25,26] and their accuracy was later criticized [27].

Acknowledgements

The authors wish to thank R. Hrach for help with calculation and modeling of the processes in the flowing afterglow. This work was supported in part by the Grant Agency of the Czech Republic under project No. 203/98/0508, and by Charles University Prague under project GA UK 179/96.

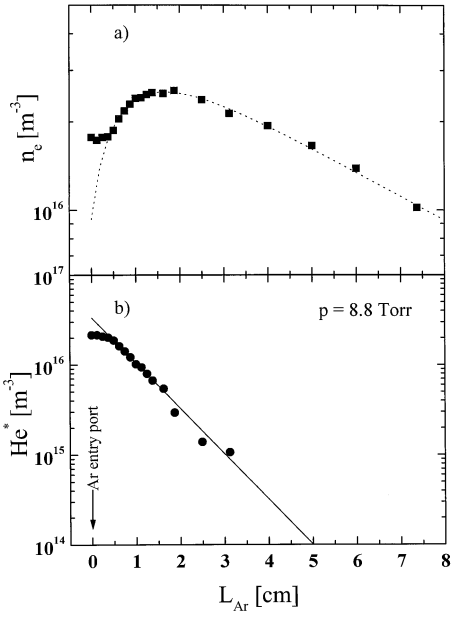

Fig. 11. (a) The evolution of the electron number density after addition of Ar. (b) The corresponding decay of the number density of He(2^3S). The pressure of the buffer gas p = 8.8 Torr. The position L_{Ar} is measured from the Ar entry port.

Appendix

Metastable atoms He(2^1S) and He(2^3S) are produced together with the charged particles produced in a He discharge (both DC and microwave) of the plasma source. More energetic He(2^1S) are converted in superelastic collisions with electrons to He(2^3S) [28]. Metastable He(2^3S) atoms are then carried along the flow tube from the discharge region and represent an important source of energy that influences relaxation of the decaying plasma. Ar gas is usually added in the post-discharge region to quench these metastables. Although this technique is commonly used, we present its detailed analysis in this Appendix to demonstrate that it is also applicable in the conditions of the HPFA apparatus.

The measurements presented here have been carried out using the DC discharge. However, there is no reason to expect very different results in the case when a microwave discharge is used. Ar has been added to the flow tube approximately 10 cm downstream of the DC discharge region; this position is denoted in related figures as $L_{\mathrm{Ar}} = 0$ (corresponding to time $t = 0$). The measured evolution of the electron number density (n_e) is plotted as a function of the position in the flow tube in Fig. 11. The fast increase of n_e is due to the production of the electrons by Penning ionization:

$$\mathrm{He}(2^3\mathrm{S}) + \mathrm{Ar} \rightarrow \mathrm{Ar}^+ + \mathrm{e}^- + \mathrm{He} \qquad (3)$$

The corresponding decay curve of the number density of the metastable atoms He(2^3S) along the flow tube can be calculated from the increase of the electron number density, n_e, plotted in the upper panel of Fig. 11. The lower panel of Fig. 11 shows this decay curve, which provides the rate coefficient of Reaction (1), $k = 7.10^{-11}$ cm^3 s^{-1} (in good agreement with the previous study by Lindinger et al. [18]). The production of the Penning electrons and correspond-

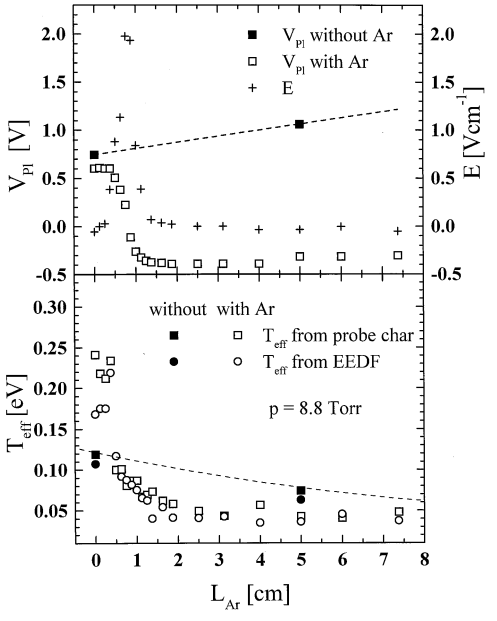

Fig. 12. The variation of the plasma potential (V_{Pl}), the intensity of the electric field (E), and the effective electron temperature (T_{eff}) along the flow tube. The effective temperature is used because the EEDF is not purely Maxwellian. The sample of data taken in pure He are indicated by the solid symbols and by the dotted lines; the data taken after the addition of Ar are indicated by the open symbols.

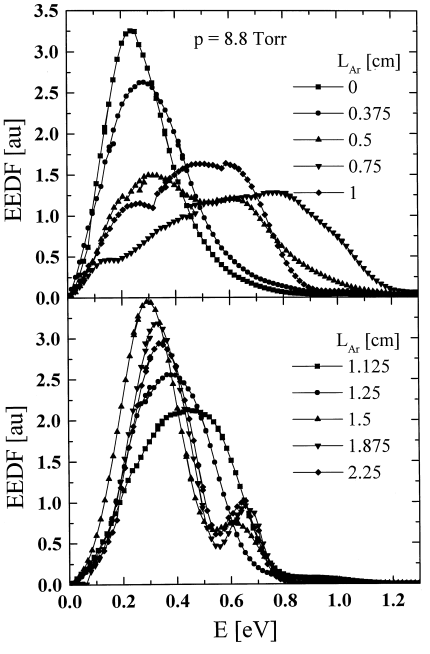

Fig. 13. The evolution of the electron energy distribution function (EEDF) in the flow tube after the addition of Ar. Note the production of high energy electrons by Penning ionization for L = 0.5–1 cm corresponding to the increase of the electron number density (see Fig. 12).

ing increase of the number density of electrons and ions are connected with the sharp change in the plasma and floating potentials (see Fig. 12). The electric field accelerates the electrons thus increasing their average energy. This increase of the energy of electrons is shown in Fig. 13 where the measured EEDF are plotted. Note that for $L \geq 0.5$ cm the energy of electrons is increasing and the EEDF is not Maxwellian; for $L > 1$ cm, electron energy starts to decrease. Note also that for $L > 1.5$ cm the EEDF contains a low energy part that is close to Maxwellian and a group of fast electrons with an energy of approximately 0.65 eV.

The most important conclusion is that for $\Delta L = 10$ cm (i.e. before reactant entry port) the afterglow plasma is fully relaxed in the HPFA instrument and the EEDF is very close to Maxwellian with $T_e = 300$ K. However, we cannot exclude formation of a small amount of Ar* metastables due to transition of excitation from other excited atoms. Measured electron temperature is slightly over 300 K and this fact can be explained simply by the presence of these metastables.

References

[1] N.G. Adams, C.R. Herd, D. Smith, J. Chem. Phys. 91 (2) (1989) 963.
[2] N.G. Adams, C.R. Herd, M. Geoghegan, D. Smith, A. Canosa, J.C. Gomet, B.R. Rowe, J.L. Queffelec, M. Morlais, J. Chem. Phys. 94 (7) (1991) 4852.
[3] N.G. Adams, Int. J. Mass Spectrom. Ion Processes 132 (1994) 1.
[4] T. Gougousi, R. Johnsen, J. Chem. Phys. 107 (1997) 2430.
[5] R. Johnsen, Int. J. Mass Spectrom. Ion Processes 81 (1987) 67.
[6] N.G. Adams, in Dissociative Recombination, B.R. Rowe et al. (Eds.), Plenum, New York, 1993.
[7] C. Rebrion-Rowe, L. Lehfaoui, B.R. Rowe, J.B.A. Mitchell, J. Chem. Phys. 108 (1998) 7185.
[8] J.B.A. Mitchell, C. Rebrion-Rowe, Int. Rev. Phys. Chem. 16 (1997) 201.
[9] J. Glosik, P. Zakouřil, V. Hanzal, V. Skalský, Int. J. Mass Spectrom. Ion Processes 149/150 (1995) 187.
[10] D. Smith, P. Španěl, Adv. At., Mol., Opt. Phys. 32 (1994) 307.
[11] J. Pavlík, J. Glosík, M. Šícha, M. Tichý, P. Potoček, Contrib. Plasma Phys. 30 (1990) 437.
[12] L.S. Frost, A.V. Phelps, Phys. Rev. 136 (1964) A1538.
[13] D. Trunec, P. Španěl, D. Smith, Contrib. Plasma Phys. 34 (1994) 69.
[14] J. Glosík, J. Pavlík, M. Šícha, Czech. J. Phys. B 33 (1983) 1230.
[15] P. Španěl, J. Glosík, Elementary Processer in Clusters, Lasers, and Plasmas (EPCLP) 91, Kühtai-Innsbruck, April 1991, pp. 252.
[16] J. Glosík, I. Čermák, M. Šícha, M. Tichý, P. Zakouřil, in W. Freysinger et al. (Eds.), 1992 International Conference on Plasma Physics (ICPP), Contributed Papers, Part III, Innsbruck, Austria, June–July 1992, pp. 1989–1992.
[17] P. Španěl, Int. J. Mass Spectrom. Ion Processes 149/150 (1995) 299.
[18] W. Lindinger, A.L. Schmeltekopf, F.C. Fehsenfeld, J. Chem. Phys. 61 (1974) 2890.
[19] P. Španěl, L. Dittrichová, D. Smith, Int. J. Mass Spectrom. Ion Processes 129 (1993) 183.
[20] J.D. Swift, M.J.R. Schwar, Electrical Probes for Plasma Diagnostics, Iliffe, London, 1970.
[21] Y. Ikezoe, S. Matsuoka, M. Takebe, A. Viggiano, Gas Phase Ion–Molecule Reaction Rate Constants, The Mass Spectroscopy Society of Japan, Tokyo, 1987.
[22] N.G. Adams, D. Smith, E. Alge, J. Chem. Phys. 81 (1984) 1778.
[23] F.J. Mehr, M.A. Biondy, Phys. Rev. 181 (1969) 264.
[24] M. Krishnamurthy, J.A. de Gouw, L. Ning Ding, V.M. Bierbaum, S.R. Leone, J. Chem. Phys. 106 (1997) 530.
[25] C.-M. Huang, M.A. Biondi, R. Johnsen, Phys. Rev. A 14 (1976) 984.
[26] C.-M. Huang, M. Whitaker, M.A. Biondi, R. Johnsen, Phys. Rev. A, 18 (1978) 64.
[27] R. Johnson, Proceedings of the 8th International Seminar on Electron and Ion Swarms, Trondheim, Norway, July 1993, p. 51.
[28] A.V. Phelps, Phys. Rev. 99 (1955) 1307.